Frequency response of spin drift-diffusion in n-doped Ge, Si, and GaAs

F. Scali,[1] M. Finazzi,[1] F. Bottegoni,[1] and C. Zucchetti[1]
Dipartimento di Fisica, Politecnico di Milano, Piazza Leonardo da Vinci 32, 20133 Milano, Italy

(*Electronic mail: francesco.scali@polimi.it)

(Dated: 13 January 2025)

The frequency dependent drift-diffusive spin transport of polarized electrons lying at the bottom of the conduction band of n-doped Ge, Si, and GaAs is numerically investigated at room temperature. First, we calculate the spin lifetime for such electron populations. Then, the temporal evolution of a spin population detected at a certain distance from the injection point is studied by employing a finite element method to solve the coupled spin drift-diffusion and continuity equations in a one-dimensional frame. In this way, we unveil the intricate dependence of the spin accumulation as a function of the distance between the injection and detection point, the doping level of the semiconductor, and the amplitude and frequency of the electric field. Notably, the spin signal features both a variation in phase with the electric field, and a modulation at higher harmonics. The cut-off frequency of the spin signal increases with the electric field's amplitude or by reducing the spin-diffusion length. With applied bias voltages compatible with those used in electronics, we obtain cut-off frequencies of about 35 GHz in Ge, 480 MHz in Si and 15 THz in GaAs. Our results not only shed light on the fundamental mechanisms governing spin dynamics but also hold the promise for future applications in spin-dependent logic operations.

I. INTRODUCTION

One of the aims of spintronics is to boost the performances of electronic devices by developing new architectures able to fast control the spin degree of freedom of carriers in solid-state systems[1,2]. Non-local (NL) geometries, where the spin injection is spatially separated with respect to the spin detection, are fundamental to manipulate the information hauled by spins thanks to the possibility of modulating the spin signal within the transport channel[3–5]. Both electrical[6,7] and optical spin injection[8–11] are exploited in NL architectures to generate spin-oriented populations in semiconductors[12,13]. Schottky tunnel contacts are used to electrically generate spin accumulation in four-terminal devices as lateral spin valves[14,15]. The modulation of a spin current can be typically performed with an external magnetic field, which induces spin precession, or with an applied electric field, that can also drive spin precession owing to the spin-orbit coupling (SOC)[16] as in spin field-effect transistors (spin-FET)[17] or similar NL transport geometries[18,19]. Nevertheless, demonstrations of spin-current modulation have thus far been restricted to electrons and holes confined to two dimensions or fewer at cryogenic temperatures[20–22] and only recently at room temperature[23]. Alternately, a spin-polarized electron population generated in the semiconductor can be accelerated or decelerated by an electric field before entering into a spin detector[24,25]. Thanks to the finite spin lifetime, the accelerating (decelerating) electric field enables spin-polarized electrons to travel longer (shorter) distances before depolarization. In this way, a spin-dependent signal can be electrically modulated at the detector even at room temperature without exploiting SOC-induced spin precession to provide either high or low output voltages from a NL device or a spin interconnect[26].

In this work, we investigate the spatial and temporal dependence of a spin-polarized electron population density $s = n_{\downarrow} - n_{\uparrow}$, being $n_{\downarrow}$ ($n_{\uparrow}$) the spin-down (up) electron density aligned along a quantization axis, subject to an electric field $E(t) = E_0 \sin(2\pi f t)$ in a one-dimensional (1D) NL geometry. Two regimes of spin drift-diffusion depending on the amplitude of the electric field are observed: i) the first one is representative of a "weak field regime" in which the spin density mostly oscillates at the modulation frequency of the field f for almost all the investigated injector-detector distances x, whereas ii) the second one is representative of a "strong field regime", occurring for larger electric field amplitudes E_0, in which a leading contribution at $2f$ appears. We evaluate the cut-off frequency for the two regimes as a function of the doping density N_d and the distance x at room temperature to identify the best-case scenario for the modulation of a spin-dependent signal exploiting spin drift-diffusion in Ge, Si, and GaAs. This study reveals the possibility to control spin-dependent output signals with high-frequency electric fields in NL architectures and spin interconnects, a critical requirement for developing fast-response spin-based logic devices in CMOS-compatible platforms. The present results and the revealed spin dynamics can also assist in guiding the time-dependent operations of semiconductor junctions displaying spin-voltaic effect[27] or spin-dependent signal amplification[28].

II. NUMERICAL SIMULATIONS

The spatial and temporal dependence of a spin-polarized electron population density $s(x,t)$ is evaluated by applying the finite element method (Comsol Multiphysics® 6.0) to numerically solve the time dependent coupled spin drift-diffusion and continuity equations, which, for a 1D geometry and an uniform electric field applied along the x-axis, read[16,29,30], re-

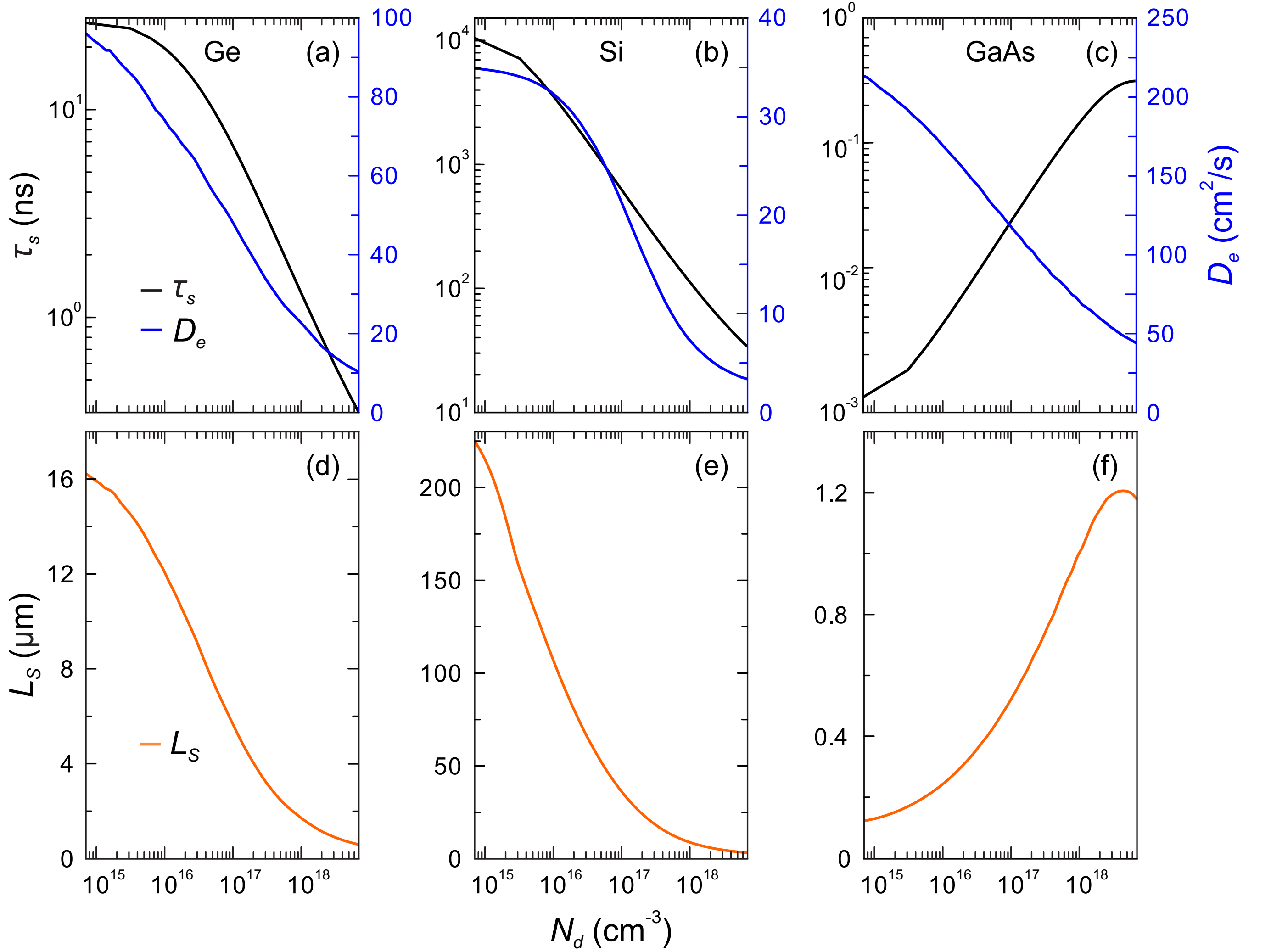

FIG. 1. (a-c) Calculated electron spin lifetime τ_s, diffusion coefficient D_e and (d-f) spin-diffusion length L_s as a function of the doping density N_d for n-doped (a-d) Ge, (b-e) Si and (c-f) GaAs at room temperature. The values of τ_s and L_s are valid for electrons lying at the bottom of the conduction band at L for Ge, Γ for GaAs and in the three Δ valleys along X for Si, as explained in the Appendix A.

spectively:

$$j_s(x,t) = q\left[\mu_e E(t)s(x,t) + D_e\frac{\partial s(x,t)}{\partial x}\right], \tag{1a}$$

$$\frac{\partial s(x,t)}{\partial t} = \frac{1}{q}\frac{\partial j_s(x,t)}{\partial x} - \frac{s(x,t)}{\tau_s}. \tag{1b}$$

In the previous expressions, $j_s(x,t)$ is the spin current density, τ_s the electron spin lifetime, q the elementary charge, μ_e the electron mobility, $E(t) = E_0\sin(2\pi f t)$ a sinusoidal time-varying electric field, $D_e = \mu_e k_B T/q$ the electron diffusion coefficient, k_B the Boltzmann constant and T the temperature. Note that Eqs. (1) describe only spin transport within the channel between the injection and the detection point. Accounting for other factors that may limit response times, such as junction capacitance at detection, are beyond the scope of this work. The doping dependence of D_e is obtained from Ref. 31–33, while the one of τ_s is calculated as described in the Appendix A (see Fig. 1a-c). The equations are solved for electrons, since spin-polarized holes in the valence band of n-doped semiconductors are characterized by a much shorter spin lifetime (of the order of femtoseconds at room temperature[34]). Furthermore, the electron-hole recombination is neglected in Eqs. (1) because it occurs on a much longer timescale compared to τ_s in Ge[35], Si[36] and GaAs[37], having a negligible impact on the spin density. The dependence of the spin-diffusion length $L_s = \sqrt{D_e\tau_s}$ (see Fig. 1d-f) is different for GaAs due to the presence of the Dyakonov-Perel spin relaxation mechanism, which is instead absent in Ge and Si (details in the Appendix A). Since L_s shows large variations as a function of the semiconductor and of the doping level, the simulations domain and the mesh-size are scaled with L_s. We consider a $10L_s$-thick segment, which guarantees that the net spin population is negligible at the end of the domain even with the applied electric field, and a mesh-size of $L_s/30$. The boundary conditions for $t > 0$ are set as $j_s(0,t) = j_0$ and $s(10L_s,t) = 0$, which represent a constant spin current at the

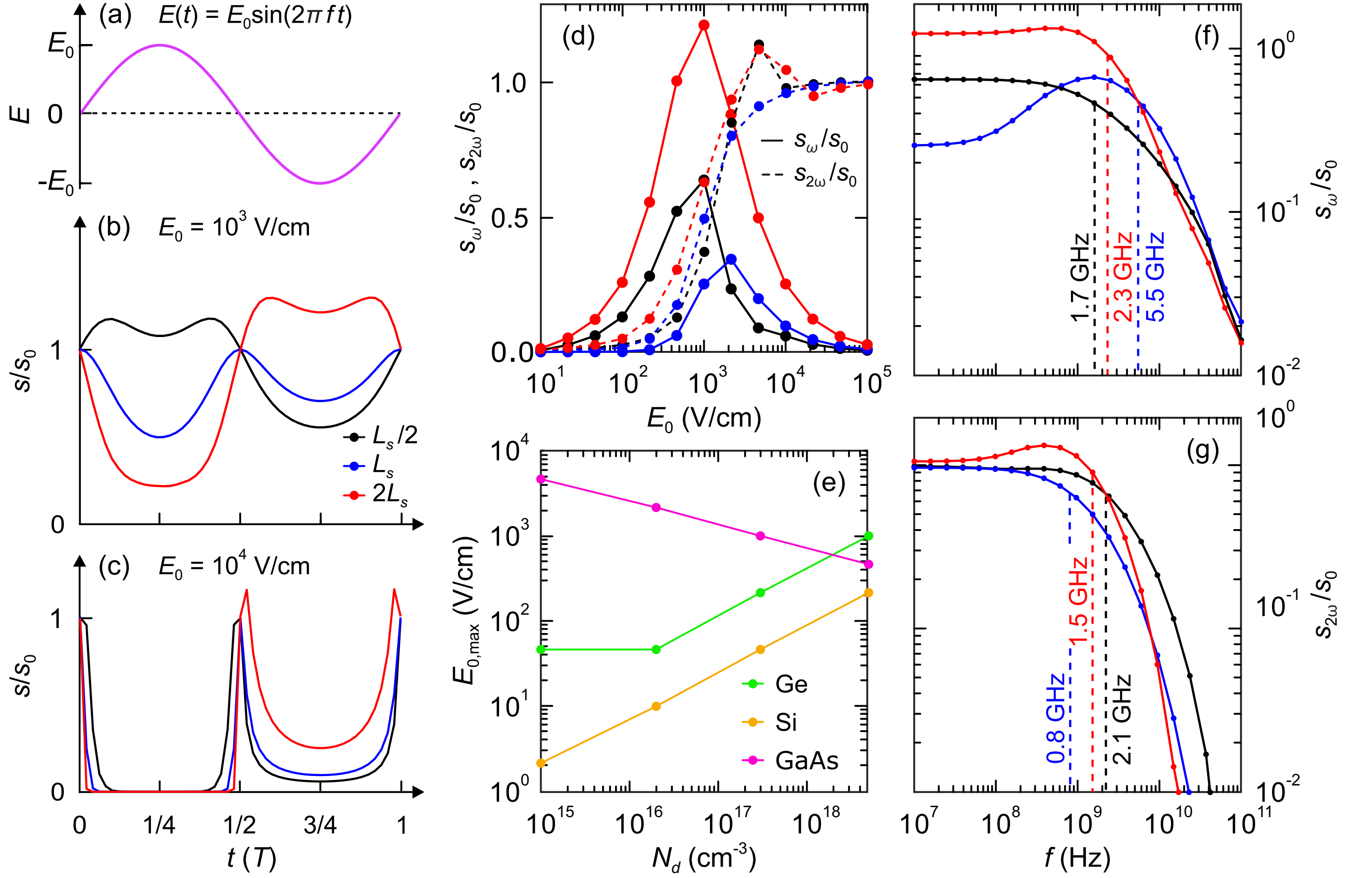

FIG. 2. Temporal dependence of the (a) sinusoidal time-varying electric field $E(t)$ and (b-c) normalized spin density s/s_0 evaluated with an amplitude of the field (b) $E_0 = 10^3$ V/cm and (c) $E_0 = 10^4$ V/cm, a modulation frequency $f = 10^7$ Hz and an injector-detector distance $x = L_s/2$ (black), $x = L_s$ (blue) and $x = 2L_s$ (red) in 5×10^{18} cm^{-3} n-doped Ge. (d) Electric field's amplitude E_0 dependence of s_ω/s_0 (solid lines) and $s_{2\omega}/s_0$ (dashed lines), i.e., the amplitudes of the first and the second harmonics of the spin density, respectively. (e) Doping density N_d dependence of $E_{0,\max}$, i.e., the E_0 value that corresponds to the maximum s_ω/s_0 in panel d, in Ge (green), Si (yellow) and GaAs (violet). (f-g) Modulation frequency f dependence of (f) s_ω/s_0 and (g) $s_{2\omega}/s_0$ evaluated in 5×10^{18} cm^{-3} n-doped Ge with $E_0 = E_{0,\max}$. The dashed vertical lines report the cut-off frequencies f_ω and $f_{2\omega}$ of s_ω and $s_{2\omega}$, respectively.

injection point and a zero spin accumulation at the end of the domain, respectively. The initial state is $s(x,0) = s_0(x) = s_0(0)e^{-x/L_s}$, which is the steady-state analytical solution of Eqs. (1) in a pure diffusive regime, i.e., for $E(t) = 0$, and in a semi-infinite space with the same left-boundary ($x = 0$) condition described before. With μ_e, D_e, τ_s and L_s provided as input parameters, Eqs. (1) are numerically solved for different amplitudes E_0 and modulation frequencies f of the electric field. The output quantity of the calculation is the spin density $s(x,t)$ normalized to the spin density in a pure diffusive regime $s_0(x)$. As a figure of merit of the modulation, we study s_ω/s_0 and $s_{2\omega}/s_0$, i.e., the normalized amplitudes of the first and the second harmonics of the spin density, respectively, as a function of E_0 and f. The cut-off frequencies f_ω and $f_{2\omega}$ for the weak and the strong field regimes are then estimated as the values satisfying $|s_\omega(x, f_\omega)| = \max(|s_\omega(x, f)|)/\sqrt{2}$ and $|s_{2\omega}(x, f_{2\omega})| = \max(|s_{2\omega}(x, f)|)/\sqrt{2}$, respectively.

III. RESULTS AND DISCUSSION

A case in point of the temporal dependence of s is shown in Fig. 2a-c. We evaluate the temporal dependence of the normalized spin density s/s_0 for a n-doped Ge substrate (5×10^{18} cm^{-3}) within a single period of the electric field (panel a) for $E_0 = 10^3$ V/cm (panel b) and $E_0 = 10^4$ V/cm (panel c). We sample the spin density for an injector-detector distance $x = L_s/2$, $x = L_s$ and $x = 2L_s$ and a frequency $f = 10^7$ Hz, which is well below the cut-off as detailed later. By varying E_0, two spin drift-diffusion regimes are distinguished. The first one for $E_0 = 10^3$ V/cm (panel b) is representative of a *weak field regime* in which s primarily oscillates at the modulation frequency and can exceed the diffusive density s_0 when $E(t) \neq 0$ and $x \neq L_s$. In this case, s is larger than s_0 when the electric field accelerates spin-polarized electrons for $x > L_s$, or when the electric field decelerates spin-polarized electrons for $x < L_s$. This is a direct consequence of the electric field pulling spin-polarized electrons far away from the injection point for $E(t) < 0$, thus favouring spin accumulation at large

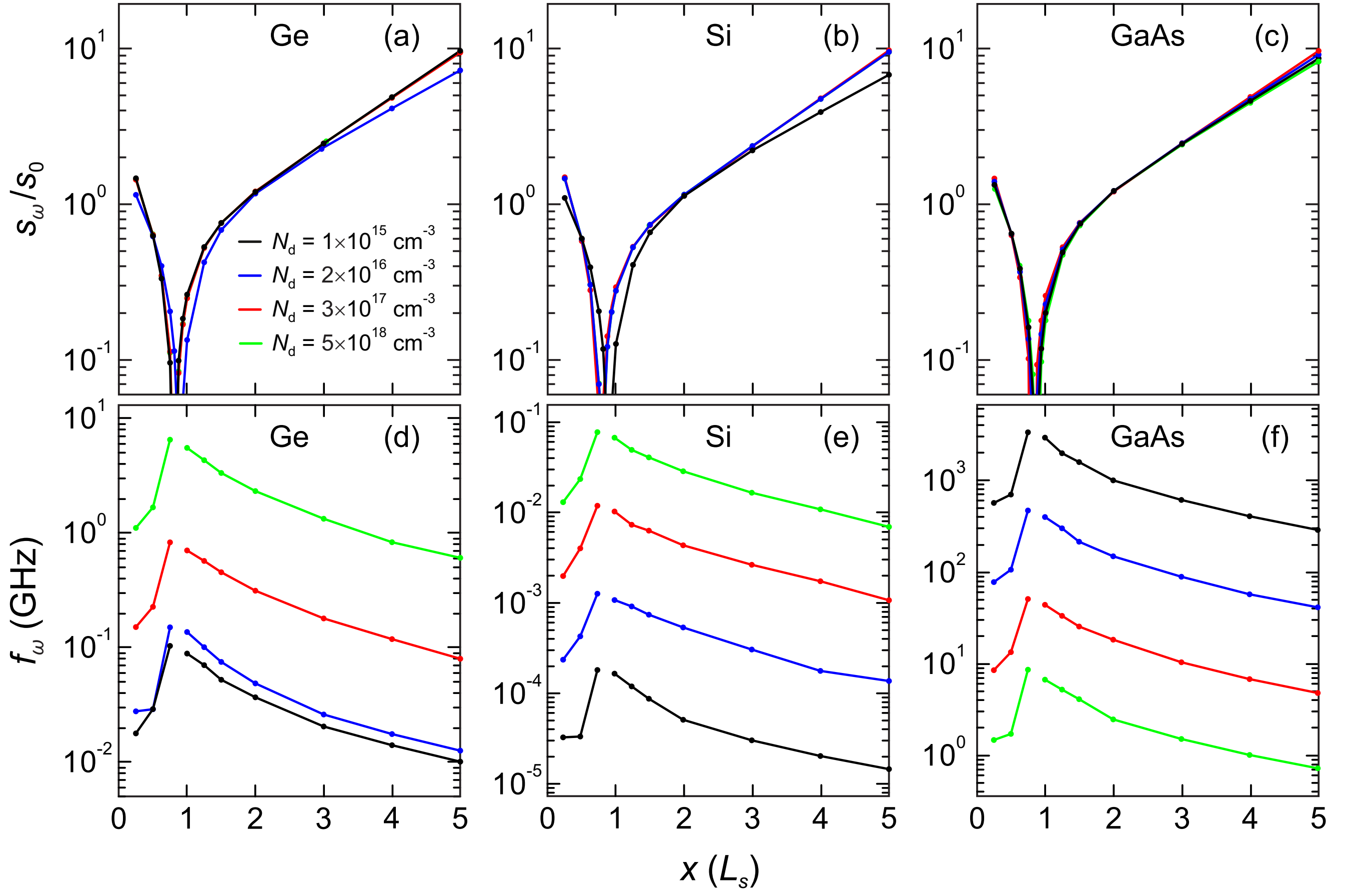

FIG. 3. (a-c) s_ω/s_0 and (d-f) f_ω as a function of injector-detector distance x for (a-d) Ge, (b-e) Si, and (c-f) GaAs. The doping density N_d ranges between 1×10^{15} cm^{-3} (black), 2×10^{16} cm^{-3} (blue), 3×10^{17} cm^{-3} (red) and 5×10^{18} cm^{-3} (green). All the data are evaluated for $E_0 = E_{0,\max}$ and s_ω/s_0 is calculated with a modulation frequency $f < f_\omega$.

distances. Instead, it confines electrons close to the injection point for $E(t) > 0$, thus favouring spin accumulation at small distances. Hence, the spin density mostly oscillates at f and $s(x \lesssim L_s,t)$ and $s(x \gtrsim L_s,t)$ are in antiphase. Notably, at $x = L_s$, the maximum spin density occurs at integer multiples of $T/2$, i.e., when $E(t) = 0$, and $s(L_s,T/2) = s_0(L_s)$. This is because a positive (negative) electric field confines spin carriers near the injection point (or pushes them away from it). This mechanism reduces the absolute number of spin carriers at $x = L_s$ regardless of the field direction, leading to oscillations at twice the modulation frequency. Instead, the second one for $E_0 = 10^4$ V/cm (panel c) is representative of a *strong field regime* in which s exhibits peaks at a repetition rate of $2f$ and remains mostly lower than s_0. In the strong field regime, both positive and negative values of $E(t)$ can reduce s with respect to s_0 because the electric field is sufficiently strong to confine electrons very close to or very far away from the injection point. Therefore, s primarily oscillates at twice the modulation frequency and is characterized by peaks located at integer multiples of $T/2$ for $x = L_s$, or lightly shifted with respect to $T/2$ for $x \neq L_s$ (see the red line in Fig. 2c as an example). The latter is explained because s can eventually increase above s_0 for a short time when $E(t) \approx 0$. The peculiar behavior for $x = L_s$ and the presence of two spin drift-diffusion regimes are consequences of the electric field influencing the average distance traveled by spin-polarized electrons before depolarizing without affecting the total amount of spin inside the domain (see Appendix B for a thorough discussion).

In the frequency domain, we evaluate s_ω and $s_{2\omega}$ for 5×10^{18} cm^{-3} n-doped Ge (see Fig. 2d) as a function of E_0. This confirms the presence of two spin drift-diffusion regimes. Indeed, s_ω dominates the spin density for $x \neq L_s$ at low E_0 and has a maximum for $E_{0,\max}$, a value that depends on the semiconductor and the doping density (see Fig. 2e). Instead, $s_{2\omega}$ represents the main contribution at $E_0 > E_{0,\max}$, therefore $E_{0,\max}$ can be considered as the electric field amplitude which separates the weak and the strong field regimes. For $x = L_s$, $s_{2\omega}$ is the leading contribution even in the weak field regime, as expected from the time domain analysis reported above. Fig. 2f-g shows an example for determining the cut-off frequencies f_ω and $f_{2\omega}$ in the frequency response of s_ω and $s_{2\omega}$, respectively, for $E_0 = E_{0,\max}$. The non-monotonic behavior of s_ω and $s_{2\omega}$ as a function of f (see the blue and the red lines in Fig. 2f and g, respectively) arises from the suppression of higher harmonics with cut-off frequencies lower with respect to f_ω and $f_{2\omega}$, thus enhancing s_ω and $s_{2\omega}$ close to their cut-off.

In the following, $E_0 = E_{0,\max}$ will be used to estimate the cut-off frequency in the weak field regime f_ω, being the field amplitude that maximizes s_ω. The bias voltage ΔV_0 that provides an electric field $E_0 = E_{0,\max}$ in the semiconductor can be estimated by considering two ohmic contacts spaced by $5L_s$ apart and assuming an uniform electric field within the semiconductor. Under these conditions, the maximum electric field corresponds to an applied ΔV_0 ranging between $200-700$ mV for Ge, Si, and GaAs depending on the doping density, which are reasonable values commonly exploited in electronic devices. Instead, $E_0 = 10\,E_{0,\max}$ will be used to estimate the cut-off frequency in the strong field regime $f_{2\omega}$ to have $s_{2\omega}$ as the leading contribution of the spin density without exploiting bias voltages larger than few volts.

The doping density and the injector-detector distance dependencies of s_ω/s_0 and f_ω, evaluated for $E_0 = E_{0,\max}$ and s_ω/s_0 for $f < f_\omega$, are reported in Fig. 3a-f. The s_ω/s_0 ratio decreases as x increases for $x \lesssim 0.8\,L_s$ (see Fig. 3a-c). It reaches a zero value around $0.8\,L_s$, where the number of accumulated spin carriers is equal for both positive and negative electric fields. Beyond $x \gtrsim 0.8\,L_s$, the s_ω/s_0 ratio increases driven by the increasing difference in the number of accumulated spin carriers for positive and negative electric fields. Ultimately, it exhibits a trend only determined by the decrease of s_0 with increasing injector-detector distance. It is worth pointing out that, except for $x \approx 0.8\,L_s$, s_ω/s_0 remains above 10% for almost all the investigated combinations of injector-detector distance, semiconductor material, and doping density. Instead, f_ω increases when L_s decreases (see Fig. 3d-f, and Appendix C for further discussion). This occurs because spin-polarized electrons must cover longer distances when their spin-diffusion length is larger to observe an electrically-driven modulation of s, slowing the response of spin accumulation to the applied field. Hence, the largest f_ω is obtained in heavily doped Ge and Si, and in lightly doped GaAs due to the opposite trends of L_s as a function of N_d. In Si, the largest f_ω is only 80 MHz. Conversely, the f_ω is about 7 GHz in Ge and larger than 2.5 THz in GaAs, owing to the significantly lower L_s with respect to Si. The doping density and the injector-detector distance dependencies of $s_{2\omega}/s_0$ and $f_{2\omega}$, evaluated for $E_0 = 10\,E_{0,\max}$ and $s_{2\omega}/s_0$ for $f < f_{2\omega}$, are reported in Fig. 4a-f. The $s_{2\omega}/s_0$ ratio remains above 100% for all the investigated distances x, also close to L_s (see Fig. 4a-c). The enhancement of $s_{2\omega}/s_0$ for $x \geq 2L_s$ and $x \leq L_s/2$ stems from the increasing of s above s_0 for $t \approx T/2$ and $E(t) \approx 0$ in the strong field regime, as discussed before. Both f_ω and $f_{2\omega}$ (see Fig. 4d-f) are maximum for $x \approx 0.75L_s$, thus where s_ω and $s_{2\omega}$ are close to the minimum, revealing a faster response for lower modulated spin accumulation. Moreover, $f_{2\omega}$ is larger than f_ω for all the investigated scenarios. This is explained because $s_{2\omega}/s_0$ dominates the spin density for larger E_0 and the latter allows to modulate at higher frequencies. In this regime, $f_{2\omega}$ is about 35 GHz in heavily doped Ge, 480 MHz in heavily doped Si and 15 THz in lightly doped GaAs. Therefore, exploiting high electric fields can dramatically improve the amplitude and the frequency response of a spin-dependent output signal.

IV. CONCLUSION

We have numerically investigated the dynamics of spin-polarized electrons in Ge, Si, and GaAs driven by a sinusoidal time-varying electric field and detected at a distance from the injection point of the order of the spin-diffusion length. The frequency response of spin drift-diffusion is characterized by two regimes depending on the amplitude of the electric field, where the first and the second harmonics of the spin density are the dominating contributions, respectively. Our simulations suggest that the strong field regime, where the second harmonic dominates, is characterized with a higher cut-off frequency with respect to the weak field regime, allowing for the exploitation of modulation frequencies up to 35 GHz in Ge, 480 MHz in Si, and 15 THz in GaAs by using modest bias voltages. These results suggest that a spin-dependent output signal can be modulated exploiting spin drift-diffusion at high frequencies in a vast range of distances between the injection and the detection point. These findings not only contribute to a better understanding of spin dynamics in semiconductors, but also pave the way to using high-frequency electric fields for fast-response spin-based logic applications in CMOS-compatible platforms.

V. ACKNOWLEDGMENT

We acknowledge funding from project SPIGA, PNRR, M4C2 investment 1.1, PRIN 2022 (Grant No. P2022LXNYN), and project MOSES, PRIN 2022 (Grant No. 20222LPKZR) founded by European Union, Next Generation EU, and the Italian Ministry of University and Research.

Appendix A: Electron spin lifetime

The doping dependence of the electron spin lifetime τ_s at room temperature, which is estimated by considering the intra- and inter-valley scattering rates with impurities and phonons[38–41] following the approach of Ref. 42, is valid for thermalized electrons, with kinetic energy $E_k = k_B T$, laying at the minima of the conduction band at the L and Γ point for Ge and GaAs, respectively, and in the three Δ valleys of the Brillouin zone for Si. The momentum-relaxation time τ_m of spin-polarized carriers related to the ionized-impurity scattering is calculated using the Brooks-Herring approach[43], whereas τ_m associated to the phonon scattering is evaluated as detailed in Ref.[43]. In Ge and Si, the spin relaxation is described within the Kane model of the Elliot-Yafet (EY) theory[44,45], which is valid for electrons at the Γ point and only approximately at the L point for Ge and in the Δ valleys for Si, yielding a τ_s proportional to τ_m[46]:

$$\tau_s^{\mathrm{EY}} = \left(\frac{\Delta_{so}}{E_g + \Delta_{so}} \frac{k_B T}{E_g} \right)^{-2} \tau_m, \tag{A-1}$$

being Δ_{so} the spin-orbit splitting and E_g the band gap. τ_m decreases by increasing the doping concentration because of

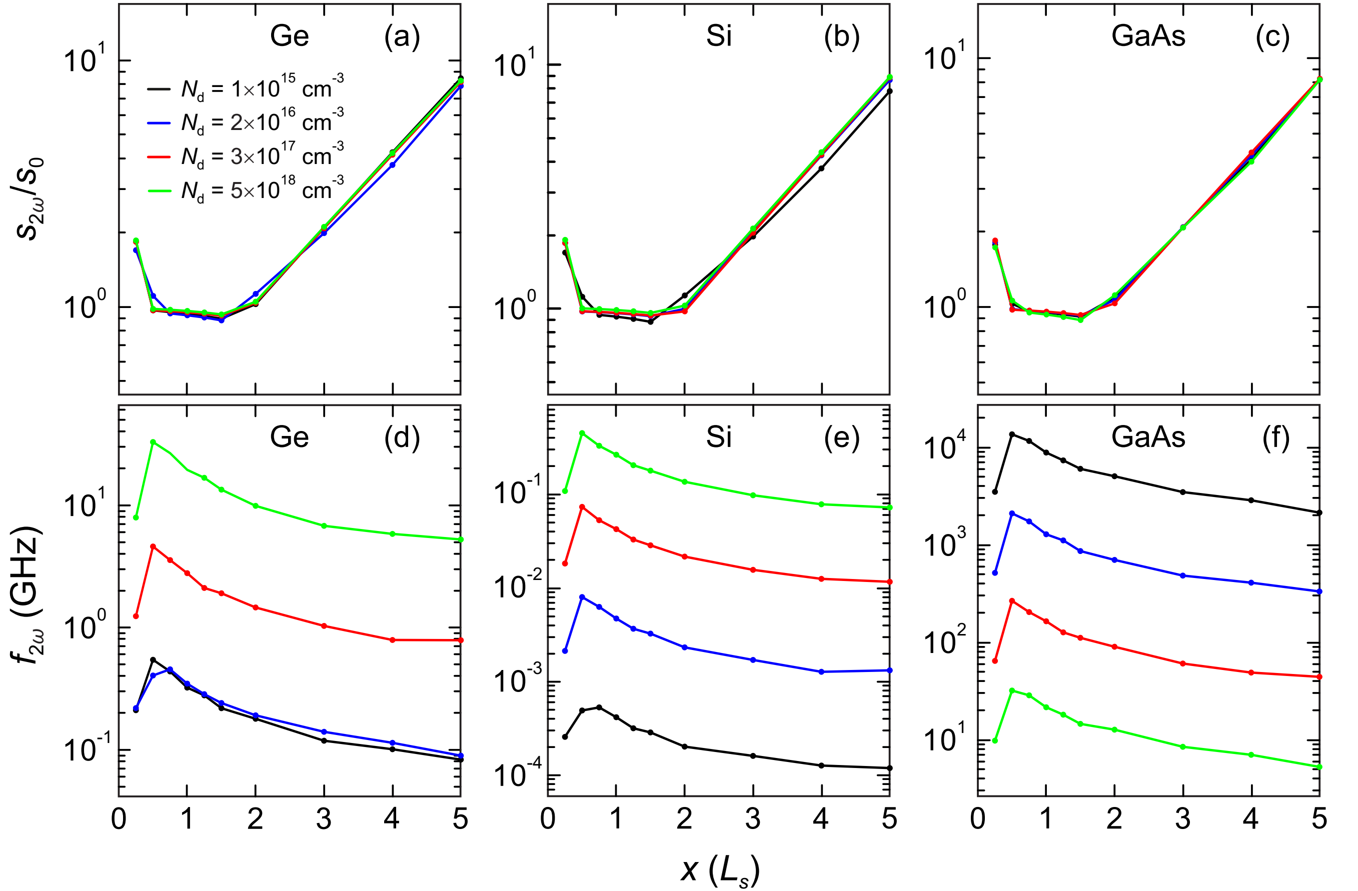

FIG. 4. (a-c) $s_{2\omega}/s_0$ and (d-f) $f_{2\omega}$ as a function of injector-detector distance x for (a-d) Ge, (b-e) Si, and (c-f) GaAs. The doping density N_d ranges between 1×10^{15} cm^{-3} (black), 2×10^{16} cm^{-3} (blue), 3×10^{17} cm^{-3} (red) and 5×10^{18} cm^{-3} (green). All the data are evaluated for $E_0 = 10\,E_{0,\max}$ and $s_{2\omega}/s_0$ is calculated with a modulation frequency $f < f_{2\omega}$.

ionized-impurity scattering[43]. Therefore, τ_s decreases with the doping density in the doping range where the impurity scattering is the leading depolarization channel, namely for $N_d > 3\times10^{16}$ cm^{-3} and $N_d > 5\times10^{15}$ cm^{-3} in Ge and Si[47,48], respectively. For lower doping concentrations, the spin lifetime is instead dominated by inter-LL (in Ge) and inter-$\Delta\Delta$ (in Si) valley scattering mediated by phonons, and results less dependent on N_d. Conversely, GaAs lacks inversion symmetry and spin depolarization is driven by the combination of the EY and the Dyakonov-Perel (DP) spin-relaxation mechanisms, with the latter that can be calculated following the Pikus and Titkov model[49]:

$$\tau_s^{\mathrm{DP}} = \left(Q\tau_m\alpha_c^2\frac{(k_BT)^3}{\hbar^2E_g}\right)^{-1}, \tag{A-2}$$

being Q a dimensionless parameter depending on the operative scattering process ($Q = 1.5$ for scattering by ionized impurities) and α_c a coefficient determining the value of the spin splitting ($\alpha_c = 0.07$ in GaAs)[49,50]. The polar optical phonon scattering[43], which is expected to be critical for momentum and spin relaxation in III-V semiconductors at 300 K[51], is evaluated as in Ref. 52 and results weaker than ionized-impurity scattering for thermalized electrons in n-doped samples. Moreover, the DP spin depolarization is more efficient than EY relaxation mechanism, thus τ_s increases with N_d revealing an opposite trend as compared to Ge and Si. Our result does not take into account the suppression of the DP spin-flip mechanism in high-mobility GaAs[50] because the electron mobility μ_e is lower than 10^4 cm^2/(V s) for whatever N_d considered here. Moreover, the metal-to-insulator transition observed near to $N_d = 2\times10^{16}$ cm^{-3} in GaAs[53], which is determinant at low-temperature, is instead negligible at room temperature and therefore disregarded in the calculations. The hot-electron effect induced by the electric field, which reduces τ_s, is also neglected being weak for the investigated doping densities and electric field amplitudes[54]. The Bir–Aronov-Pikus relaxation mechanism is not considered in our estimations of τ_s in Ge, Si, and GaAs because in n-doped semiconductors there are few holes and the electron-hole exchange interaction is negligible[29]. Our spin lifetime τ_s in Ge and GaAs is in accordance with previous reports[47,53–57], whereas it is larger with respect to Refs. 58 and 59 in Si. This discrepancy could be ascribed to the tough application of the Kane model for electrons in the Δ-valleys[48,60], leaving out the inter-valley spin-flip mechanism driven by impurity scattering[58], which is only considered as an intra-valley process. Despite the large

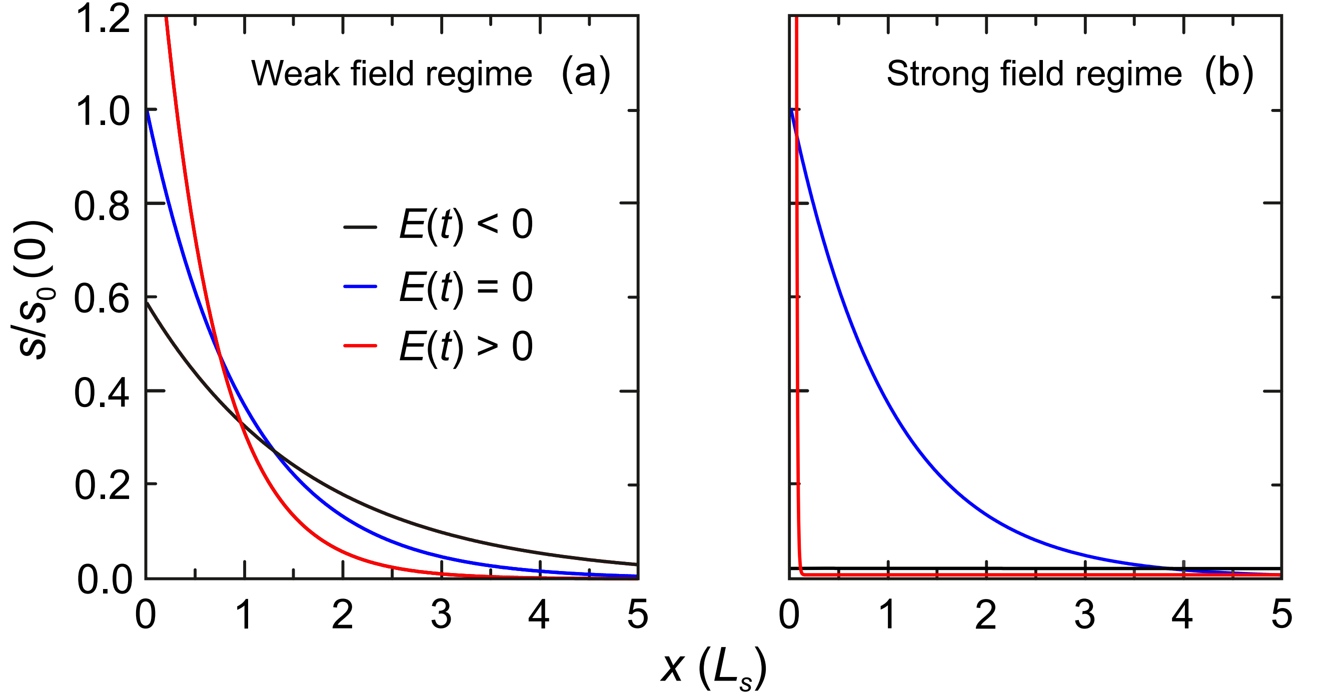

FIG. 5. Dependence of the normalized spin density $s/s_0(0)$ as a function of injector-detector distance x in the (a) weak and the (b) strong field regime for $E(t) < 0$ (black), $E(t) = 0$ (blue) and $E(t) > 0$ (red).

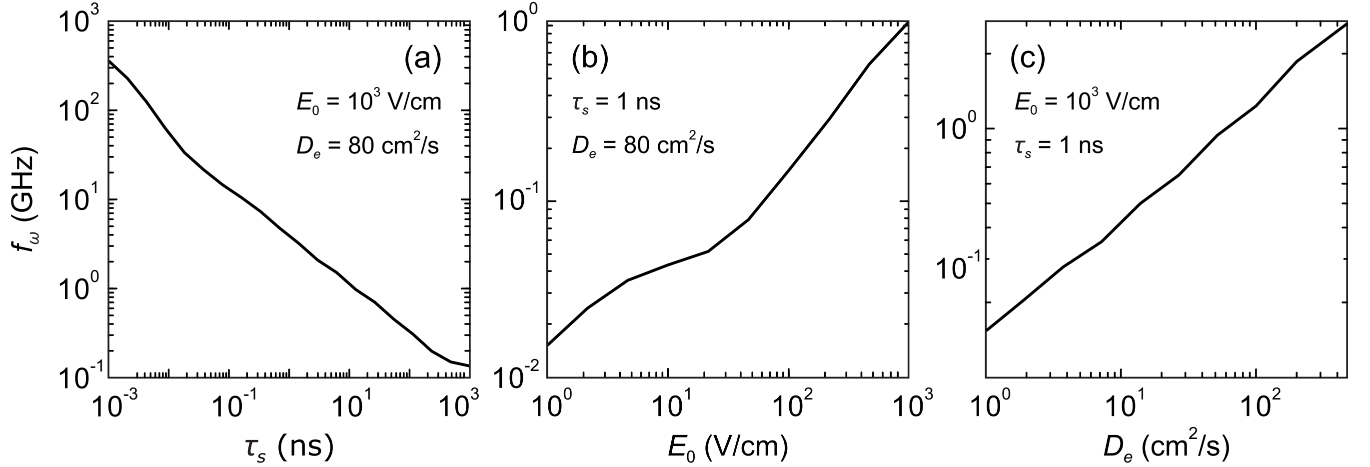

FIG. 6. Dependence of the cut-off frequency f_ω as a function of (a) electron spin lifetime τ_s, (b) electric field amplitude E_0 and (c) electron diffusion coefficient D_e evaluated at a distance $x = 2L_s$ from the injection point. Each dependence is calculated by varying each single parameter keeping the others constant and equal to $\tau_s = 1$ ns, $E_0 = 10^3$ V/cm and $D_e = 80$ cm^2/s, respectively.

number of parameters involved and the uncertainty surrounding each of them, the spin-diffusion length is in good agreement with experimental measurements (which also exhibit significant data variability) for Ge, Si, and GaAs[4,7,14,15,25,55]. In the case of Si, the agreement is within a factor of 3.

Appendix B: Conservation of the total spin in the domain

To gain insights into the temporal dependence of s/s_0 reported in Fig. 2b-c, we consider a semi-infinite domain with a fixed spin current source at the left boundary ($x = 0$) and a homogeneous electric field applied to the domain. The analytical solution of the spin accumulation is[24,25,61]:

$$s = \bar{A}e^{-x/\bar{L}_s}, \tag{A-1}$$

where $\bar{A}$ and $\bar{L}_s$ represent the amplitude and the spin transport length[25], respectively, both of which depend on the applied electric field. In the case of $E(t) = 0$, the amplitude $\bar{A}$ and the spin transport length $\bar{L}_s$ reduce to the purely diffusive values A, i.e., in the main text $s_0(0)$, and L_s. Therefore, at any $t > 0$,

the spin accumulation at $x = L_s$ is:

$$s(L_s,t) = \bar{A}e^{-L_s/\bar{L}_s}, \tag{A-2}$$

which at $t = 0$, when $E(t) = 0$, simplifies to $s(L_s,0) = A/e$. Hence:

$$\frac{s(L_s,t)}{s(L_s,0)} = \frac{\bar{A}}{A}e^{1-L_s/\bar{L}_s}. \tag{A-3}$$

Since the application of an electric field does not affect the source and sink terms in Eqs. (1), the total spin s_{tot} accumulated in the domain is conserved between $t = 0$ and any $t > 0$. By integrating Eq. (A-1) over the entire domain, we find that $s_{\text{tot}} = \bar{A}\bar{L}_s$. Since this also equals to AL_s at $t = 0$, the conservation of s_{tot} gives $AL_s = \bar{A}\bar{L}_s$, and Eq. (A-3) can be expressed as:

$$\frac{s(L_s,t)}{s(L_s,0)} = \frac{L_s}{\bar{L}_s}e^{1-L_s/\bar{L}_s}. \tag{A-4}$$

This expression has an absolute maximum at $\bar{L}_s = L_s$, where $s(L_s,t) = s(L_s,0)$, meaning that the application of either a positive or negative electric field reduces the spin accumulation at $x = L_s$ compared to the purely diffusive case. Conversely, as shown in Fig. 5a-b, the application of an electric field can either increase or decrease the accumulated spin compared to the purely diffusive scenario for $x \neq L_s$.

Appendix C: Trends for the best operating condition

Since an analytical expression of f_ω can not be obtained, we isolate the dependencies of f_ω at room temperature with respect to τ_s, E_0 and D_e by varying each single parameter and keeping the others constant to determine which are the best conditions to operate. The dependencies are reported for $x = 2L_s$ to avoid the peculiar case of $x = L_s$ discussed in the main text. As shown in Fig. 6a, f_ω decreases with τ_s, which indicates that the modulation driven by spin drift-diffusion is more effective when spin-polarized electrons depolarize faster. This can be explained because the spin-diffusion length increases with the spin lifetime, resulting in a slower response of the spin accumulation to the electric field. In Fig. 6b, f_ω increases with E_0 as a consequence of a larger driving force able to displace spin-polarized carriers in the domain, suggesting the possibility of increasing the cut-off frequency exploiting larger fields. Finally, f_ω increases with D_e, and therefore with μ_e, in Fig. 6c. This occurs because high-mobility spin-polarized electrons are characterized by larger velocities which enable faster modulation. In conclusion, operating with large electric fields on high-mobility electrons with low spin lifetime enhances the response of spin drift-diffusion.

[1] I. Žutić, J. Fabian, and S. Das Sarma, "Spintronics: Fundamentals and applications," Rev. Mod. Phys. **76**, 323–410 (2004).
[2] D. Awschalom and M. E. Flatté, "Challenges for semiconductor spintronics," Nat. Phys **3**, 153–159 (2007).
[3] K. Y. Camsari, S. Ganguly, and S. Datta, "Modular approach to spintronics," Sci. Rep. **5**, 10571 (2015).
[4] C. Zucchetti, F. Bottegoni, C. Vergnaud, F. Ciccacci, G. Isella, L. Ghirardini, M. Celebrano, F. Rortais, A. Ferrari, A. Marty, M. Finazzi, and M. Jamet, "Imaging spin diffusion in germanium at room temperature," Phys. Rev. B **96**, 014403 (2017).
[5] T. Guillet, C. Zucchetti, A. Marchionni, A. Hallal, P. Biagioni, C. Vergnaud, A. Marty, H. Okuno, A. Masseboeuf, M. Finazzi, F. Ciccacci, M. Chshiev, F. Bottegoni, and M. Jamet, "Spin orbitronics at a topological insulator-semiconductor interface," Phys. Rev. B **101**, 184406 (2020).
[6] M. Yamada, M. Tsukahara, Y. Fujita, T. Naito, S. Yamada, K. Sawano, and K. Hamaya, "Room-temperature spin transport in n-Ge probed by four-terminal nonlocal measurements," Appl. Phys. Express **10**, 093001 (2017).
[7] F. Rortais, C. Vergnaud, A. Marty, L. Vila, J. P. Attané, J. Widiez, C. Zucchetti, F. Bottegoni, H. Jaffrès, J. M. George, and M. Jamet, "Non-local electrical spin injection and detection in germanium at room temperature," Appl. Phys. Lett. **111**, 182401 (2017).
[8] F. Bottegoni, M. Celebrano, M. Bollani, P. Biagioni, G. Isella, F. Ciccacci, and M. Finazzi, "Spin voltage generation through optical excitation of complementary spin populations," Nat. Mater **13**, 790–795 (2014).
[9] F. Bottegoni, G. Isella, S. Cecchi, and F. Ciccacci, "Spin polarized photoemission from strained Ge epilayers," Appl. Phys. Lett. **98** (2011).
[10] F. Bottegoni, C. Zucchetti, G. Isella, E. Pinotti, M. Finazzi, and F. Ciccacci, "Modeling the photo-induced inverse spin-Hall effect in Pt/semiconductor junctions," J. Appl. Phys. **124** (2018).
[11] A. Marchionni, C. Zucchetti, F. Ciccacci, M. Finazzi, H. S. Funk, D. Schwarz, M. Oehme, J. Schulze, and F. Bottegoni, "Inverse spin-Hall effect in GeSn," Appl. Phys. Lett. **118** (2021).
[12] C. Zucchetti, F. Scali, A. Ballabio, M. Bollani, G. Isella, G. Ferrari, M. Finazzi, F. Ciccacci, and F. Bottegoni, "Hole and electron spin lifetime in lightly n-doped silicon at low temperatures," Appl. Phys. Lett. **125** (2024).
[13] F. Scali, C. Zucchetti, L. Anzi, V. Falcone, and F. Bottegoni, "Photo-induced inverse spin Hall effect detection of spin-polarized holes in semiconductors," in *Spintronics XVII*, Vol. 13119 (SPIE, 2024) pp. 48–55.
[14] O. M. J. Van't Erve, A. T. Hanbicki, M. Holub, C. H. Li, C. Awo-Affouda, P. E. Thompson, and B. T. Jonker, "Electrical injection and detection of spin-polarized carriers in silicon in a lateral transport geometry," Appl. Phys. Lett. **91**, 212109 (2007).
[15] M. Ciorga, A. Einwanger, U. Wurstbauer, D. Schuh, W. Wegscheider, and D. Weiss, "Electrical spin injection and detection in lateral all-semiconductor devices," Phys. Rev. B **79**, 165321 (2009).
[16] J. Fabian, A. Matos-Abiague, C. Ertler, P. Stano, and I. Žutić, "Semiconductor spintronics," Acta Phys. Slovaca **57** (2007).
[17] S. Datta and B. Das, "Electronic analog of the electro-optic modulator," Appl. Phys. Lett. **56**, 665–667 (1990).
[18] J. H. Smet, R. A. Deutschmann, F. Ertl, W. Wegscheider, G. Abstreiter, and K. Von Klitzing, "Gate-voltage control of spin interactions between electrons and nuclei in a semiconductor," Nat. **415**, 281–286 (2002).
[19] C. Morrison, P. Wiśniewski, S. D. Rhead, J. Foronda, D. R. Leadley, and M. Myronov, "Observation of Rashba zero-field spin splitting in a strained germanium 2D hole gas," Appl. Phys. Lett. **105** (2014).
[20] S. Gardelis, C. G. Smith, C. H. W. Barnes, E. H. Linfield, and D. A. Ritchie, "Spin-valve effects in a semiconductor field-effect transistor: A spintronic device," Phys. Rev. B **60**, 7764 (1999).
[21] A. Balocchi, Q. H. Duong, P. Renucci, B. L. Liu, C. Fontaine, T. Amand, D. Lagarde, and X. Marie, "Full electrical control of the electron spin relaxation in GaAs quantum wells," Phys. Rev. Lett. **107**, 136604 (2011).
[22] P. Chuang, S. C. Ho, L. W. Smith, F. Sfigakis, M. Pepper, C. Chen, J. C. Fan, J. P. Griffiths, I. Farrer, H. E. Beere, *et al.*, "All-electric all-semiconductor spin field-effect transistors," Nat. Nanotechnol **10**, 35–39 (2015).
[23] P. A. Dainone, N. F. Prestes, P. Renucci, A. Bouché, M. Morassi, X. Devaux, M. Lindemann, J. M. George, H. Jaffrès, A. Lemaitre, *et al.*, "Controlling the helicity of light by electrical magnetization switching," Nat. **627**, 783–788 (2024).
[24] C. Zucchetti, A. Marchionni, M. Bollani, F. Ciccacci, M. Finazzi, and F. Bottegoni, "Electric field modulation of spin transport," APL Mater. **10**, 011102 (2022).
[25] C. Zucchetti, F. Scali, P. Grassi, M. Bollani, L. Anzi, G. Isella, M. Finazzi, F. Ciccacci, and F. Bottegoni, "Non-local architecture for spin current manipulation in silicon platforms," APL Mater. **11**, 021102 (2023).
[26] H. Dery, Y. Song, P. Li, and I. Žutić, "Silicon spin communication," Appl. Phys. Lett. **99** (2011).

[27] I. Žutić, J. Fabian, and S. Das Sarma, "Spin-polarized transport in inhomogeneous magnetic semiconductors: theory of magnetic/nonmagnetic p-n junctions," Phys. Rev. Lett. **88**, 066603 (2002).
[28] J. Fabian, I. Žutić, and S. Das Sarma, "Magnetic bipolar transistor," Appl. Phys. Lett. **84**, 85–87 (2004).
[29] I. Žutić, J. Fabian, and S. Das Sarma, "Spin injection through the depletion layer: A theory of spin-polarized p-n junctions and solar cells," Phys. Rev. B **64**, 121201 (2001).
[30] I. Žutić, J. Fabian, and S. C. Erwin, "Spin injection and detection in silicon," Phys. Rev. Lett. **97**, 026602 (2006).
[31] V. I. Fistul, M. I. Iglitsyn, and E. M. Omelyanovskii, "Mobility of electrons in germanium strongly doped with arsenic," Sov. Phys. Solid State **4**, 784–785 (1962).
[32] M. Sotoodeh, A. H. Khalid, and A. A. Rezazadeh, "Empirical low-field mobility model for III−V compounds applicable in device simulation codes," J. Appl. Phys. **87**, 2890–2900 (2000).
[33] C. Jacoboni, C. Canali, G. Ottaviani, and A. A. Quaranta, "A review of some charge transport properties of silicon," Solid-State Electron. **20**, 77–89 (1977).
[34] F. Rortais, S. Oyarzún, F. Bottegoni, J. C. Rojas-Sánchez, P. Laczkowski, A. Ferrari, C. Vergnaud, C. Ducruet, C. Beigné, N. Reyren, *et al.*, "Spin transport in p-type germanium," J. Condens. Matter Phys. **28**, 165801 (2016).
[35] R. N. Hall, "Electron-hole recombination in germanium," Phys. Rev. **87**, 387 (1952).
[36] J. A. del Alamo and R. M. Swanson, "Modelling of minority-carrier transport in heavily doped silicon emitters," Solid-State Electron. **30**, 1127–1136 (1987).
[37] C. J. Hwang, "Doping dependence of hole lifetime in n-type GaAs," J. Appl. Phys. **42**, 4408–4413 (1971).
[38] M. V. Fischetti, "Monte Carlo simulation of transport in technologically significant semiconductors of the diamond and zinc-blende structures. I. Homogeneous transport," IEEE Trans. Electron Devices **38**, 634–649 (1991).
[39] M. V. Fischetti and J. M. Higman, "Theory and Calculation of the Deformation Potential Electron-Phonon Scattering Rates in Semiconductors," in *Monte Carlo Device Simulation: Full Band and Beyond* (Springer US, 1991) pp. 123–160.
[40] M. H. Kuok, S. C. Ng, Z. L. Rang, and D. J. Lockwood, "Acoustic phonon dispersion at hypersonic frequencies in Si and Ge," Phys. Rev. B **62**, 12902–12908 (2000).
[41] M. H. Kuok, S. C. Ng, V. L. Zhang, and D. J. Lockwood, "Acoustic mode dispersion at hypersonic frequencies in GaAs," Solid State Commun. **116**, 27–31 (2000).
[42] C. Zucchetti, F. Bottegoni, G. Isella, M. Finazzi, F. Rortais, C. Vergnaud, J. Widiez, M. Jamet, and F. Ciccacci, "Spin-to-charge conversion for hot photoexcited electrons in germanium," Phys. Rev. B **97**, 125203 (2018).
[43] M. Lundstrom, "Fundamentals of carrier transport, 2nd edn," Meas. Sci. Technol. **13**, 230–230 (2002).
[44] R. J. Elliott, "Spin-Orbit Coupling in Band Theory—Character Tables for Some "Double" Space Groups," Phys. Rev. **96**, 280 (1954).
[45] Y. Yafet, "g Factors and spin-lattice relaxation of conduction electrons," in *Solid State Phys.*, Vol. 14 (Elsevier, 1963) pp. 1–98.
[46] C. Guite and V. Venkataraman, "Temperature dependence of spin lifetime of conduction electrons in bulk germanium," Appl. Phys. Lett. **101**, 252404 (2012).
[47] P. Li, Y. Song, and H. Dery, "Intrinsic spin lifetime of conduction electrons in germanium," Phys. Rev. B **86**, 085202 (2012).
[48] J. L. Cheng, M. W. Wu, and J. Fabian, "Theory of the spin relaxation of conduction electrons in silicon," Phys. Rev. Lett. **104**, 016601 (2010).
[49] F. Meier and B. P. Zakharchenya, *Optical orientation* (Elsevier, 2012).
[50] R. I. Dzhioev, K. V. Kavokin, V. L. Korenev, M. V. Lazarev, N. K. Poletaev, B. P. Zakharchenya, E. A. Stinaff, D. Gammon, A. S. Bracker, and M. E. Ware, "Suppression of Dyakonov-Perel spin relaxation in high-mobility n-GaAs," Phys. Rev. Lett. **93**, 216402 (2004).
[51] A. Dyson and B. K. Ridley, "Spin relaxation in cubic III−V semiconductors via interaction with polar optical phonons," Phys. Rev. B **69**, 125211 (2004).
[52] S. Oertel, J. Huebner, and M. Oestreich, "High temperature electron spin relaxation in bulk GaAs," Appl. Phys. Lett. **93** (2008).
[53] R. I. Dzhioev, K. V. Kavokin, V. L. Korenev, M. V. Lazarev, B. Y. Meltser, M. N. Stepanova, B. P. Zakharchenya, D. Gammon, and D. S. Katzer, "Low-temperature spin relaxation in n-type GaAs," Phys. Rev. B **66**, 245204 (2002).
[54] J. H. Jiang and M. W. Wu, "Electron-spin relaxation in bulk III−V semiconductors from a fully microscopic kinetic spin Bloch equation approach," Phys. Rev. B **79**, 125206 (2009).
[55] C. Zucchetti, M. Bollani, G. Isella, M. Zani, M. Finazzi, and F. Bottegoni, "Doping dependence of the electron spin diffusion length in germanium," APL Mater. **7**, 101122 (2019).
[56] F. Bottegoni, C. Zucchetti, F. Ciccacci, M. Finazzi, and G. Isella, "Optical generation of pure spin currents at the indirect gap of bulk Si," Appl. Phys. Lett. **110**, 042403 (2017).
[57] H. Kurebayashi, T. Trypiniotis, K. Lee, S. Easton, A. Ionescu, I. Farrer, D. A. Ritchie, J. A. C. Bland, and C. H. W. Barnes, "Electrical determination of the spin relaxation time of photoexcited electrons in GaAs," Appl. Phys. Lett. **96** (2010).
[58] Y. Song, O. Chalaev, and H. Dery, "Donor-driven spin relaxation in multivalley semiconductors," Phys. Rev. Lett. **113**, 167201 (2014).
[59] T. Suzuki, T. Sasaki, T. Oikawa, M. Shiraishi, Y. Suzuki, and K. Noguchi, "Room-temperature electron spin transport in a highly doped Si channel," Appl. Phys. Express **4**, 023003 (2011).
[60] P. Li and H. Dery, "Spin-orbit symmetries of conduction electrons in silicon," Phys. Rev. Lett. **107**, 107203 (2011).
[61] Z. G. Yu and M. E. Flatté, "Electric-field dependent spin diffusion and spin injection into semiconductors," Phys. Rev. B **66**, 201202 (2002).